Materials Science & Engineering A 597 (2014) 279–287

Contents lists available at ScienceDirect

Materials Science & Engineering A

journal homepage: www.elsevier.com/locate/msea

A rate dependent constitutive model for ECAE Cu based on instrumented nanoindentation results

J. Su [a,b], W.G. Guo [b], L.J. Kecskes [c], S.N. Mathaudhu [c], Q. Wei [a,*]

[a] Department of Mechanical Engineering, University of North Carolina at Charlotte, Charlotte, NC 28223-0001, USA
[b] School of Aeronautics, Northwestern Polytechnical University, Xi'an, Shaanxi 710072, People's Republic of China
[c] WMRD, US Army Research Laboratory, Aberdeen Proving Ground, MD 21005-5069, USA

ARTICLE INFO

Article history:
Received 1 November 2013
Received in revised form
20 December 2013
Accepted 28 December 2013
Available online 7 January 2014

Keywords:
Equal channel angular extrusion
Copper
Constitutive model
Rate effect
Nanoindentation

ABSTRACT

We have investigated the plastic deformation behavior, especially the strain rate sensitivity of Cu, subjected to severe plastic deformation via equal channel angular extrusion (ECAE) with a varying number of passes. We have performed nanoindentation strain rate jump experiments to measure the hardness values at different loading rates, and determine the strain rate sensitivity (SRS). In turn, the activation volume (V^*) associated with plastic deformation of the ECAE Cu has been derived and analyzed. Based on the dislocation-mediated processes during ECAE, including dislocation accumulation, dynamic recovery and recrystallization, combined with creep theory, a strain rate dependent constitutive model has been constructed for the ECAE Cu. We have reached good agreement between the model predictions and the experimental results. It was found that the model can provide a plausible understanding of the various aspects of the mechanical behavior of the ECAE Cu.

1. Introduction

Severe plastic deformation (SPD) is one of several efficient processes to refine grain size and to obtain ultrafine-grained (UFG, grain size, d, smaller than 1000 nm, but greater than 100 nm) and nanocrystalline (NC, $d < 100$ nm) materials. Different forms of SPD such as equal channel angular pressing or extrusion (ECAP or ECAE) [1], accumulative roll-bonding (ARB) [2], high-pressure torsion (HPT) [3] etc. have been widely utilized both in industry and research laboratories. Estrin et al. [4] gave a brief review of the various SPD techniques in the diamond jubilee issue of Acta Materialia to recount the historic milestones in this area. As one of the most popular SPD techniques, ECAE has been demonstrated to be highly efficient in improving the strength with a relatively small loss of ductility by refining the grain size. Numerous articles have been published since Segal [5] invented the technique in 1977 and was granted a US patent in 1996. The basic operating conditions such as those of pure and simple shear, the total strain, equivalent strain during each pass using different route orientations, and deformation mode and history have been extensively enumerated [6–11]. Since then, many research groups have made further contributions to the development of the ECAE technique. Azushima [12], Valiev [13], and Zhu [14], for example, have developed the basic theoretical understanding, articulated the currently accepted technical extrusion routes and, more broadly, various applications of the different SPD processes to produce UFG metals and alloys. The key properties of SPD processed nanostructured materials have been evaluated and tabulated, including their fundamental physical parameters (diffusivity, elasticity, and internal friction), mechanical properties (strengthening behavior, ductility, fatigue, and super-plasticity), and other physical and engineering properties (magnetic hysteresis, optical properties of semiconductors, and corrosion behavior) and the potential practical applications have been discussed. Many authors [2,15–27] have published on the SPD processing of metals, particularly, using the ECAE technique. These investigations include copper, nickel, aluminum, titanium, tantalum, iron, tungsten, niobium, as well as many alloys. Specifically, processing induced microstructural evolution and structure-property relationships have been examined.

However, there are still many unresolved and outstanding issues that remain, particularly associated with the deformation mechanisms of UFG/NC metals produced by various SPD techniques. As such, efforts to achieve better and deeper understanding of the mechanical behavior of these SPD processed UFG metals and alloys have been continued. Significant progress has been made with the help of advanced techniques such as transmission electron microscopy (TEM), electron backscatter diffraction (EBSD), or orientation imaging microscopy (OIM). For example, EBSD analysis has shown that the fraction of high angle grain boundaries (HAGBs) of ECAE Nb and Cu continue to increase with

* Corresponding author. Tel.: +1 704 687 8213; fax: +1 704 684 8345.
E-mail address: qwei@uncc.edu (Q. Wei).

0921-5093/$ - see front matter © 2014 Elsevier B.V. All rights reserved.
http://dx.doi.org/10.1016/j.msea.2013.12.090

total equivalent strain, even though the apparent grain size reduction saturates quickly after a few passes [28–30]. EBSD has also provided information on other important microstructural features of SPD materials such as the average grain size, grain size distribution, and texture evolution. In other studies, TEM examinations have helped to clarify our understanding of the grain size reduction mechanisms by delineating the processes of grain division and dislocation density evolution with increased equivalent strain [31–34]; a more quantitative evaluation has also been performed [35].

Despite the large number of on-going and past efforts and publications on SPD of UFG/NC metals and alloys, a literature survey suggests that so far, little progress has been made on documenting the constitutive behavior of these materials. In the past, various constitutive models have been proposed or developed to describe the plastic flow behavior of metallic materials. The list of the more popular models includes the Johnson–Cook model [36], the Zerilli–Armstrong model [37], the mechanical threshold stress (MTS) model by Follansbee and Kocks [38], the Bodner–Partom [38] (B–P model), a physics-based model proposed by Nemat–Nasser [39–41], and many others enumerated in References [42–50]. While nearly all these models are applicable for the coupled effect of strain rate and temperature, they have been developed, more or less, specifically for the high strain rate regime. Basically, these constitutive models can be classified into three groups.

1.1. Empirical models

The mathematical forms of the empirical constitutive models, such as the Johnson–Cook model [36], the Voce-type equations [51,52], etc. are relatively simple. It is also relatively easy to uncouple and single out all the model parameters. However, the disadvantages of these empirical models are that there is no physical meaning of the original equations, even though some of the terms have been given physical meaning during later development and derivation (for example, the Voce-type equations) [51–53]. Owing to their simple forms and ease to be incorporated into a computer code, these models have been widely used in engineering and industrial simulations and modeling.

1.2. Physics-based models

These models, such as the Zerilli–Armstrong model [37], the MTS model [38], the Nemat-Nasser model (physics-based as claimed by the authors) [39], the V–A model by Vojiadjis and Abed [44–46,54], are constructed based on a common assumption, that is the flow stress can be considered as the combination of the athermal component (related to the long-range dislocation barriers, such as grain boundaries, far field forest dislocation, and other far field factors) and the thermal activation component (related to the short-range barriers, such as Peierls–Nabarro potential, vacancies and solute atoms and other point defects, etc.). In these physics-based constitutive models, the athermal stress component is insensitive to temperature, while the thermal activation component is strongly dependent on temperature and strain rate.

1.3. Bodner–Partom (B–P) and Zener–Hollomon (Z–H) models

The B–P model, which was formulated by Bodner and Partom [42,55] based on phenomenological considerations and continuum mechanics, describes the elastic–plastic strain hardening behavior of materials for large deformations and arbitrary loading histories. The typical feature of this model is that the deformation rate is separated into elastic and inelastic components, and they are functions of state variables at all stages of loading and unloading. In addition, the Zener–Hollomon parameter (Z-parameter) [56,57] reflects the relationship between strain rate and temperature with an activation energy. Later on Sellars and Tegart [58] proposed a relationship between the Z-parameter and the flow stress based on creep theory, and eventually constructed the Zener–Hollomon constitutive model.

However, compared with coarse-grained metals, mechanical properties of SPD UFG metals exhibit certain peculiar characteristics such as higher flow stress, lower strain-hardening rate, changed strain rate sensitivity [59], etc., brought about by the SPD processes. All of these features are associated with the microstructural evolution of UFG metals subjected to SPD. Therefore, the constitutive models described above may not be entirely applicable to SPD UFG metals. As such, further simulations and modeling efforts are needed to describe the constitutive behavior of these materials.

Based on the dislocation accumulation and annihilation theory, Mecking and Kocks [51] have pursued a constitutive model, and then Estrin and Mecking (E–M) [52] further developed this model to make it suitable for both dynamic loading and creep. In the E–M model, a steady state is reached by a dynamic balance between athermal work hardening (associated with the accumulation or storage of dislocations) and strain rate/temperature dependent work softening (associated with dislocation annihilation). Both the efforts of Mecking and Kocks and Estrin and Mecking were to assign physical meaning to the Voce-type equation. Since then, the Voce-type equation has been utilized to describe the constitutive behavior of UFG metals [32,60] at low to moderate equivalent strain levels. However, with further increase of equivalent strain, softening cannot be fully described by dynamic recovery alone. As such, an alternative mechanism has been proposed for rapid deformation-induced strain softening, i.e., the recrystallization process. In the construction of a constitutive model, a combination between the Voce-type equation and Avrami equation has been widely utilized at prescribed strain rates and temperatures [53,61,62]. In addition, Shafiei and Ebrahimi [63] have further proposed some new equations for modeling single peak dynamic recrystallization (DRX) flow curves.

In this paper, based on nanoindentation strain rate jump experiments, the mechanical behavior has been measured as a function of strain rate and strain for Cu that has been subjected to ECAE up to 32 passes. A strain-rate dependent constitutive model has been constructed based on these results.

2. Material processing and nanoindentation experiments

Commercially pure Cu was subjected to ECAE of increasing number of passes. The die angles of Φ and Ψ of the ECAE tool were both 90°. The specimen billets were processed via route E in the sense of Barber et al. [64]. Using this route, there is a 180° rotation between the first and second passes, and then a 90° rotation between the second and third passes, and another 180° rotation between the third and fourth passes. The first two passes are equivalent to the first two passes of route C. The billets were processed to 1, 2, 4, 8, 12, 16, 20, 24, 28, and 32 passes.

All of the ECAE processed specimens were polished by diamond lapping discs with an equivalent grit size of 30, 15, 9, 6, 3, 1, 0.5, and 0.1 μm. They were finally polished by a γ-alumina polishing powder suspension with a particle size of 0.05 μm. In order to remove the polishing powder residue from the specimen surface, the specimens were cleaned in an ultrasonic bath.

Instrumented nanoindentation experiments were performed on an Agilent G-200 Nanoindentation system (Agilent Corporation, Santa Clara, CA). Nanoindentation strain rate jump experiments were

conducted at four different strain rates (0.001, 0.004, 0.019 and 0.08/s) and for each strain rate condition 10 test points were collected. Therefore, the average hardness value at different strain rates can be obtained at a prescribed equivalent strain. Care and caution were exercised when using instrumented nanoindentation to probe the mechanical properties, particularly strain rate sensitivity of the metals [65].

3. Strain rate sensitivity and activation volume of plastic deformation

In what follows, we will provide brief descriptions of the strain rate sensitivity and activation volume associated with plastic deformation of a visco-plastic material, particularly in the context of indentation experiments. Then, we will present the nanoindentation results of the ECAE processed Cu.

3.1. Basic theory and background of strain rate sensitivity and activation volume

A significant component in constructing the constitutive equation of a material is the strain rate sensitivity factor m; m is the finger print for the thermodynamics and kinetics of plastic deformation, which, in turn, sheds light on the nature of the deformation mechanism. A detailed derivation process of the strain rate sensitivity and activation volume is developed in this section.

The Arrhenius equation, which demonstrates the temperature dependence of the kinetics, or reaction rate, can be used to describe the plastic deformation as a function of temperature and deformation rate. In view of this fact, the deformation rate $\dot{\gamma}$ can be expressed by

$$\dot{\gamma} = \dot{\gamma}_0 \exp\left(-\frac{\Delta G(\tau^*)}{kT}\right), \tag{1}$$

where $\Delta G(\tau^*)$ is the activation energy, which can be further divided into two parts [66].

$$\Delta G(\tau^*) = \Delta G^* - \tau^* V^*. \tag{2}$$

In Eq. (2), ΔG^* represents the energy required by thermal activation alone in the absence of an externally applied stress, and V^* is the thermal activation volume. In turn, this means that this volume, swept out by a dislocation line during thermal activation with the assistance of stress, may be usually given in units of b^3 (where b is the Burgers vector of dislocations).

From Eq. (2), we have

$$V^* = -\frac{\partial \Delta G(\tau^*)}{\partial \tau^*}. \tag{3}$$

Combined with Eq. (1), the activation volume then is derived to be

$$V^* = -\frac{\partial \Delta G(\tau^*)}{\partial \tau^*} = kT\frac{\partial \ln \dot{\gamma}}{\partial \tau^*}. \tag{4}$$

In addition, the strain rate sensitivity in the context of a power law rate dependence is defined as

$$m = \frac{\partial \ln \sigma}{\partial \ln \dot{\varepsilon}}. \tag{5}$$

Considering the von Mises theory, viz. $\sigma_y = \sqrt{3}\tau_y$ and $\gamma_y = \sqrt{3}\varepsilon_y$, and using the relation between hardness and yield stress in the context of Tabor's formula $H = C\sigma_y$ [67] (the constraint factor C is usually taken to be $\sim$3.0 for metals), a relationship between strain rate sensitivity and thermal activation volume can be derived in terms of hardness as

$$V^* = kT\frac{\partial \ln \dot{\gamma}}{\partial \tau^*} = \frac{kT}{\tau^*}\frac{\partial \ln \dot{\gamma}}{\partial \ln \tau^*} = \frac{\sqrt{3}kT}{\sigma m}, \tag{6a}$$

and

$$m = \frac{\sqrt{3}kT}{\sigma V^*}. \tag{6b}$$

Therefore, the activation volume for plastic deformation can be given as

$$V^* = \frac{\sqrt{3}CkT}{Hm} \tag{7}$$

Generally speaking, there have been three primary experimental methods to measure the strain rate sensitivity: strain rate jump test under compression, tension, and nanoindentation, stress relaxation, and stress–strain response at different strain rates. Details of the experimental setup and the formulas for the calculation of strain rate sensitivity values can be found in the literature [66,68–73].

3.2. Experimental results

From the nanoindentation experimental results of the ECAE Cu, the relation between hardness and the number of passes (or equivalent strain) has been established and is shown in Fig. 1(a). With a number of increasing ECAE passes, the hardness of Cu first increases rapidly, reaches its peak around four passes, followed by a general softening behavior with higher number of ECAE passes. For example, if we take the hardness at a strain rate of 0.001/s, the maximum hardness is 1.75 GPa after four ECAE passes, while the hardness of the specimen is 1.59 GPa after 32 passes. This trend is similar for all strain rates. In Fig. 1(b) the hardness of the ECAE Cu is re-plotted in terms of the applied strain rate, displaying the strong effect of strain rate on the hardness of the ECAE Cu with different equivalent strains induced by ECAE. In this figure, the same tendency has been shown with strain rate ranging from 0.001/s to 0.08/s. That is, the hardness peaks at a strain of $\sim$5.0 and it then decreases with increased equivalent strain until saturation.

In Figs. 2 and 3, the calculated SRS and activation volume are plotted, based on the experimental nanoindentation results. The following observations can be made:

(1) For ECAE Cu, the strain rate sensitivity is a function of the ECAE equivalent strain, and there is an increasing tendency of SRS with equivalent strain. The minimum SRS value is $\sim$0.026, which is attained after four ECAE passes, while the maximum SRS value is 0.033, attained after 24 passes.
(2) When the number of passes is less than eight, the activation volume of plastic deformation decreases with ECAE equivalent strain. However, it stabilizes at $\sim 24.61b^3$, especially for large numbers of ECAE passes.

4. Construction of the constitutive model

In what follows, we will attempt to develop a rate dependent constitutive model for the ECAE processed Cu of this work. First, we will describe the factors that influence the constitutive behavior of the material.

It is self-evident that as the number of passes increase, the equivalent strain imparted to the material also increases. The flow stress of the material is controlled by three competing mechanisms: the strain hardening process by dislocation multiplication, accumulation and storage, and dynamic recovery and dynamic recrystallization that are generally regarded as softening processes.

It is well know that the strain hardening component is related to the blocking effect of various barriers to prevent dislocation motion. These are grain boundaries, sessile dislocations including super-jogs, or Lomer–Cottrell locks. The effect of these mechanisms may lead to

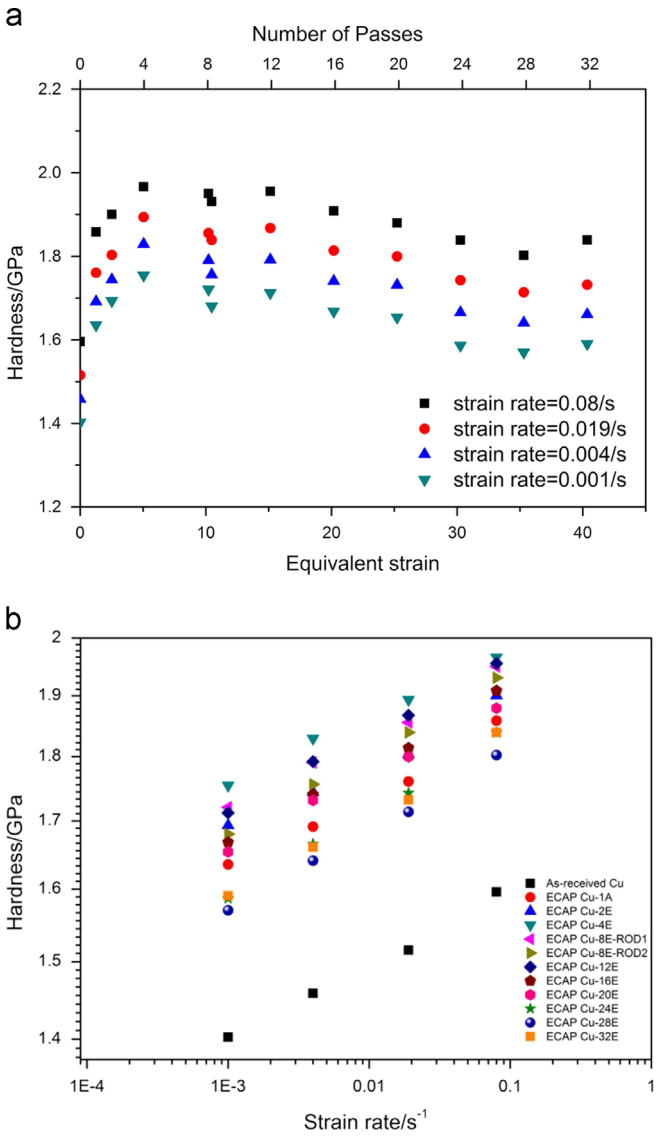

Fig. 1. Hardness as functions of the equivalent strain (or equal channel angular extrusion pass number [N]) and the strain rate obtained from the anoindentation results. (a) The hardness rapidly increases to a peak value at N=4, and then it plateaus out, and starts to decrease slightly with a further increase in N. The hardness at a given strain rate (i.e., 0.001/s for example) scales and depends on N. The equivalent strain was calculated using the equation proposed in References [1,7]. That is, $\varepsilon_N = (N/\sqrt{3})[2cot((\Phi/2)+(\Psi/2))+\Psi cosec((\Phi/2)+(\Psi/2))]$ (in our work, Φ and Ψ are both 90°). (b) Nanoindentation hardness of the ECAE Cu as a function of the indentation strain rate. The hardness values measured at different indentation strain rates are a strong function of the equivalent strain induced by ECAE as well. Note that the strain rate is plotted on a logarithmic scale.

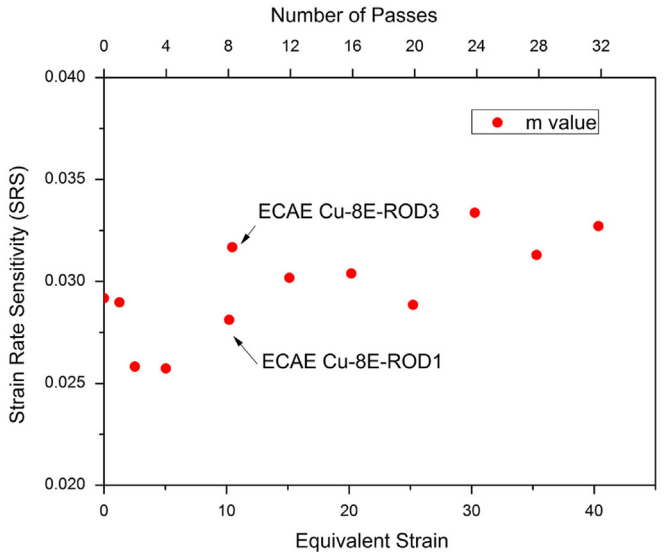

Fig. 2. The strain rate sensitivity, m, which was obtained from the equation $m = (\partial \ln H/\partial \ln \dot{\varepsilon})$, is a function of the number of ECAE passes or the equivalent strain. A generally increasing trend for the strain rate sensitivity (SRS) with N is observed from the results in, particularly when $N > 4$.

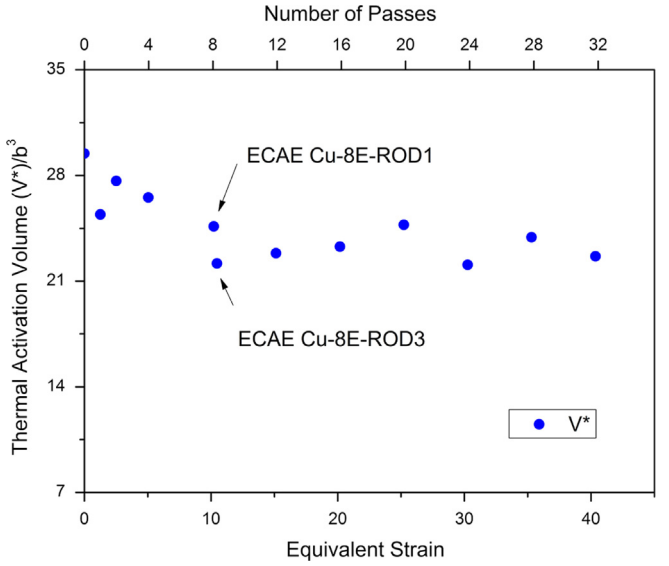

Fig. 3. The activation volume (normalized by b^3, b being the Burgers vector of the dislocation) of plastic deformation as a function of the number of ECAE passes or the equivalent strain. One can see that the activation volume first decreases slightly with N. However, at relatively large N, it starts to stabilize and this trend is unchanged up to 32 passes. In the calculation process, the Tabor factor, C=3, is utilized; that is, we have used the relation $V^* = \frac{\sqrt{3}CkT}{Hm} = \frac{3\sqrt{3}kT}{Hm}$.

dislocation accumulation. As for dynamic recovery, Gourdet and Montheillet [74] pointed out that it occurs in two ways: the condensation of dislocations into new low angle grain boundaries (LAGBs) and the absorption of the dislocations in the pre-existing boundaries which leads to the formation of sub-grain boundaries. Note, the sub-grains may eventually be transformed into HAGBs. As pointed out by Doherty et al. [75], there are two main reasons for the central importance of a recrystallization process during plastic deformation: the first is that dynamic recrystallization (DRX) softens the material and restores its ductility during low temperature deformation; the second is that it determines and controls the grain structure of the final product, whereby it is the only process to produce a completely new microstructure, including a new grain size, morphology, and orientation or texture. As such, DRX is likely the only method to obtain a new grain structure in a severe plastic deformation process. Combined with the experimental evidence for the transformation from LAGBs to HAGBs, a conclusion can be drawn that DRX is the primary mechanism responsible for the increase in grain misorientation during the severe plastic deformation processes. Furthermore, according to Gourdet and Montheillet [76], recrystallization is primarily related to grain boundary migration, which is driven by local dislocation density differences. Gleiter [77] has derived some basic theory and a calculation method for obtaining the grain boundary migration (GBM) rate.

Figs. 1 and 2 suggest that the flow stress is sensitive to strain rate. Therefore, to construct the constitutive model of the plastic

behavior of ECAE copper, the effect of strain rate should also be considered beyond the important aspects of dislocations discussed above. The detailed description will be provided in the following.

4.1. Strain hardening and dynamic recovery

It is well understood that the nature of strength of a metal during plastic deformation is rooted in its resistance to dislocation motion, which may be influenced by various factors. For pure metals, dislocation density, ρ, becomes an important variable affecting its plastic strength, and it can be expressed by the Hirsch–Bailey relation or Taylor formula:

$$\sigma = \sigma_0 + \alpha G b \rho^{1/2}, \tag{8}$$

where σ_0 is the yield stress of the material in the well-annealed condition (with a very low dislocation density), α is a geometrical factor (for an fcc material, it can be taken as 0.25), G is the shear modulus of the material (for copper, $G=80$ GPa), and b is the Burgers vector (for copper, $b \approx 0.235$ nm).

The evolution of the dislocation density has two contributions, and can be written as [51]:

$$\frac{d\rho}{d\varepsilon} = C_1 \rho^{1/2} - C_2 \rho, \tag{9}$$

where C_1 and C_2 are the material parameters. The first term of Eq. (9) is related to the athermal storage of moving dislocations which becomes immobile after moving a constant distance (dislocation accumulation), and the second term is associated with dynamic recovery which is a thermally activated process and leads to dislocation annihilation. C_2 is usually strain rate and temperature dependent.

In the Kocks–Mecking (K–M) model [52], the assumption that the mean free path of dislocations is proportional to $\rho^{1/2}$ is abandoned, especially in particle strengthened and very fine-grained materials. In this case, Eq. (9) becomes the Laasraoui–Jonas equation [61].

$$\frac{d\rho}{d\varepsilon} = C - C_2 \rho, \tag{10}$$

where the parameter C is determined from the mean free path, L, of dislocations, specifically, $C=(bL)^{-1}$, and can be considered as the hardening coefficient; C_2 is the recovery coefficient.

Combining Eqs. (8) and (10), we then have:

$$\frac{d\sigma^2}{d\varepsilon} = C(\alpha G b)^2 \left[1 - \frac{C_2}{C}\rho\right] = C(\alpha G b)^2 \left[1 - \left(\frac{\sigma}{\sigma_s}\right)^2\right]. \tag{11}$$

$$\sigma_s = \alpha G b \left(\frac{C}{C_2}\right)^{1/2}. \tag{12}$$

Then, integration of Eq. (11) gives

$$\frac{\sigma^2 - \sigma_s^2}{\sigma_0^2 - \sigma_s^2} = \exp[-\beta\varepsilon]. \tag{13}$$

In Eq. (13) σ_0 is the initial stress. Considering the extent of the severe deformation produced by each cumulative ECAE pass, the flow stress of the as-received specimen may be chosen as the value of σ_0; $\beta=C_2$ is a material constant related to strain rate and temperature, and may be determined from experimental results; σ_s corresponds to the stress level that could be attained during the work hardening regime in the absence of any additional softening effects except dynamic recovery and, thus, it may be considered as the peak stress value of the stress-strain curves. Additionally, it may be noted that the value of σ_s is also dependent on strain rate and temperature.

4.2. Dynamic recrystallization

The conventional Voce-type equations (the K–M and E–M models, for example) have been derived and given their physical meaning (i.e., the balance between work hardening and dynamic recovery based on dislocation accumulation and/or annihilation). As a result, these types of constitutive equations enable us to describe the steady state of the flow stress only [32,51,52,60,78]. For metals with relatively low melting points such as Cu, the DRX part should be included when considering the softening processes. Here we use the factor X_s, which arises from discussions of strain softening by some investigators [53,62,79]. This part is also dependent on the strain rate, and can be given as

$$X_s = \frac{\sigma_{wh} - \sigma}{\sigma_{wh} - \sigma_{sat}}, \tag{14}$$

where σ_{wh} is the flow stress predicted by the hardening equation (13), and σ_{sat} is the final saturation stress.

Considering that the softening kinetics can be described by the Avrami-type equation [61,79], and according to Oudin et al. [62], the following equation may be used

$$X_s = 1 - \exp\left[-r\left(\frac{\varepsilon}{\varepsilon_p}\right)^q\right], \tag{15}$$

where ε_p is the strain corresponding to the peak stress, and it can be identified from the stress–strain curve, r and q are constants, which are related to the softening rate and kinetics. The softening rate increases with increasing q; r is associated with the rate of softening to reach the steady state where a dynamic balance between hardening and softening has been achieved.

Incorporating Eqs. (14) and (15), a combined equation for the flow stress can be obtained which contains the strain hardening mechanisms based on dislocation activities and an empirical softening factor

$$\begin{aligned}\sigma &= \sigma_{wh} - (\sigma_{wh} - \sigma_{sat})X_s \\ &= \sigma_{wh} - (\sigma_{wh} - \sigma_{sat})\left(1 - \exp\left[-r\left(\frac{\varepsilon}{\varepsilon_p}\right)^q\right]\right) \\ &= \sigma_{sat} + (\sigma_{wh} - \sigma_{sat})\exp\left[-r\left(\frac{\varepsilon}{\varepsilon_p}\right)^q\right].\end{aligned} \tag{16}$$

4.3. Strain rate effect

Based on creep theory, Sellars and Tegart [58] proposed a correlation between strain rate and flow stress for hot-deformed materials with the following equation:

$$\dot{\varepsilon} = A(\sinh \alpha\sigma)^{n'} \exp\left(-\frac{Q}{RT}\right), \tag{17}$$

where $\dot{\varepsilon}$ is the strain rate, α, A and n' are constants, independent of temperature; Q is the activation energy; and T is the absolute temperature. In addition, a reduced exponential relationship has been delineated for different stress level regimes.

For high stress levels:

$$\dot{\varepsilon} = A''\exp(\lambda\sigma)\exp\left(-\frac{Q}{RT}\right). \tag{18a}$$

For low stress levels:

$$\dot{\varepsilon} = A'\sigma^{n'}\exp\left(-\frac{Q}{RT}\right), \tag{18b}$$

where A', A'', and $\lambda = \alpha n'$ are material constants dependent on the stress level.

In this work, we borrow the creep equation proposed by Sellars and Tegart [58], given by Eq. (17). We have simplified it for high

stress condition, and then obtained the relation between stress and strain rates, and an equivalent form of Eq. (18a) is obtained

$$\sigma = \frac{1}{\lambda}\ln\dot{\varepsilon} + \frac{1}{\lambda}\left(\frac{Q}{RT} - \ln A''\right). \tag{19}$$

From the form of this equation, therefore, we can propose that the flow stress is linearly related to the logarithmic strain rate at prescribed temperatures and stress levels, as

$$\sigma_i = \xi_i \ln\dot{\varepsilon} + \eta_i. \tag{20a}$$

The parameter $\xi_i = (1/\lambda)$ can be considered to reflect the strain rate sensitivity at different strain levels, defined as $(1/\lambda) = (\partial\sigma/\partial\ln\dot{\varepsilon})$, which more or less bears similar spirit to the definition of strain rate sensitivity ($m = (\partial\ln\sigma/\partial\ln\dot{\varepsilon})$). The intercept η_i ($\eta_i = (1/\lambda)((Q/RT) - \ln A'')$) can be considered as a stress constant related to the plastic equivalent strain. In this equation, η_i represents the flow stress value when the strain rate approaches 1/s, that is, when $ln\dot{\varepsilon} = 0$.

In our linearized constitutive model, the flow stress, σ_i with subscript i represent the various different stress levels, such as σ_s, σ_0 or σ_{sat}. The corresponding parameters ξ_i and η_i can be determined from the experimental results at the various stress levels.

4.4. The final constitutive model

Based on the aforementioned notion of dislocation evolution (strain hardening, dynamic recovery, etc.), and considering the roles of dynamic recrystallization and rate effects, the final form of the constitutive model may be obtained by substituting into Eq. (16) the values of the variables given by Eq. (20a),

$$\begin{aligned}\sigma &= \sigma_{sat} + (\sigma_{wh} - \sigma_{sat})\exp\left[-r\left(\frac{\varepsilon}{\varepsilon_p}\right)^q\right] \\ &= \xi_{sat}\ln\dot{\varepsilon} + \eta_{sat} + [\sigma_{wh} - (\xi_{sat}\ln\dot{\varepsilon} + \eta_{sat})]\exp\left[-r\left(\frac{\varepsilon}{\varepsilon_p}\right)^q\right].\end{aligned} \tag{21a}$$

$$\begin{aligned}\sigma_{wh} &= \sqrt{\sigma_s^2 + (\sigma_0^2 - \sigma_s^2)exp[-\beta\varepsilon]} \\ &= \sqrt{(\xi_s ln\dot{\varepsilon} + \eta_s)^2 + [(\xi_0 ln\dot{\varepsilon} + \eta_0)^2 - (\xi_s ln\dot{\varepsilon} + \eta_s)^2]exp[-\beta\varepsilon]}.\end{aligned} \tag{22a}$$

In this model, the parameters σ_0, σ_s and σ_{sat} represent the flow stress at the initial stage, the peak value and the final saturation state in the stress versus equivalent strain curves, respectively; σ_{wh} is the flow stress considering strain hardening and dynamic recovery, as predicted in Eq. (13). ε_p is the equivalent strain corresponding to the peak stress, and it can also be directly determined from the experimental results. In this work, $\varepsilon_p = 5$. As demonstrated in a previous section, r and q are constants related to the softening rate and kinetics. These two parameters can be identified by fitting the experimental results at different strain rates. In addition, ξ_i and η_i are two sets of derivative parameters that describe the relation between strain rates and flow stress.

5. Discussion

In what follows, we will attempt to validate the constitutive model we have constructed for the ECAE Cu, and discuss the significance of the various parameters associated with the model and within the context of the plastic deformation of ECAE Cu.

5.1. Strain rate sensitivity (SRS/m) and activation volume (V*)

The hardness of the ECAE Cu first increases with the number of passes ($N < 4$), but then decreases and then saturates with further increase in the number of passes up to 32 passes, as shown in Fig. 1(a). However, our results, shown in Figs. 2 and 3, indicate that the strain rate sensitivity has a tendency of continuously increasing with the number of passes, while the activation volume approaches a constant value ($V^* = 24.61b^3$). As noticed by other investigators [28,29,32], there is no apparent grain refinement as the number of passes exceeds a certain value during ECAE. At this point and onward, the primary microstructure evolution is associated with the recrystallization process that mainly affects grain misorientation. That is, an increasing number of low angle grain boundaries (LAGBs) are transformed into high angle grain boundaries (HAGBs).

Wei et al. [59,66,80] have presented a preliminary model for thermally activated dislocation-based processes for fcc metals. They pointed out that the strain rate sensitivity can be related to the yield stress. In the equation for the yield stress, τ, which has the following form,

$$\tau = \tau_0 + \left(\alpha\sqrt{\rho} + \frac{\beta}{\sqrt{d}}\right), \tag{23}$$

the first term is related to the lattice friction; the second is related to the Taylor contribution (forest hardening in the sense of Eq. [8] of this work), and the third one arises from the Hall–Petch relation. The parameters of α and β are associated with the evolution of microstructure, such as the amount of plastic strain, grain boundary misorientation angle, etc. In [74], based on the theory that the flow stress depends on the dislocation density, ρ_i, inside subgrains and subgrain size or dislocation density, ρ_{LAB}, within the LAGBs, the yield stress can be rewritten as

$$\tau = Gb(A_1\sqrt{\rho_i} + A_2\sqrt{\rho_{LAB}}), \tag{24}$$

where G is the shear modulus, A_1 and A_2 are constants, and ρ_i is the dislocation density inside the sub-grains. While $\sqrt{\rho_{LAB}}$ is the dislocation density within the LAGBs, and considering the fraction of LAGBs and HAGBs in the material, the ρ_{LAB} and $\overline{\theta}$ can be related by [74]

$$\rho_{LAB} = \frac{2nf_{LAB}\overline{\theta}}{bD}. \tag{25}$$

and

$$\overline{\theta} = \frac{1}{f_{LAB}}\int_{\theta_0}^{\theta_c}\varphi(\theta)\theta d\theta. \tag{26}$$

$$f_{HAB} + f_{LAB} = 1. \tag{27}$$

In these equations, f_{LAB} and f_{HAB} are the fraction of LAGBs and HAGBs; $\varphi(\theta)$ is the distribution function of LAGBs; θ and $\overline{\theta}$ are the grain orientation of LAGBs and the average grain misorientation, respectively; θ_0 is the angle at which LAGBs form, while θ_c is a critical value, above which the misorientation between two adjacent crystallites can no longer be accommodated by a dislocation wall. And, the value of θ_0 and θ_c can be chosen as 1 and 15 degrees, respectively. D is the average crystallite size, and n represents the number of dislocation sets in the boundary.

Based on the assumption that the crystallite size is more or less constant at large strain deformations, there is a balance between the area of LAGBs created during a strain increment and the area annihilated by the movement of HAGBs. As such, an important equation can be derived [74] that describes the distribution of the misorientation angle

$$\varphi(\theta) = \varphi(\theta_0)exp[-\varphi(\theta_0)(\theta - \theta_0)], \tag{28}$$

where $\varphi(\theta_0) = (\alpha/((1-\alpha)\theta_0))$.

Further, the fraction of HAGBs and the mean misorientation angle can be derived:

$$f_{HAB} = 1 - f_{LAB} = 1 - \int_{\theta_0}^{\theta_c} \varphi(\theta) d\theta = exp[-\varphi(\theta_0)(\theta_c - \theta_0)] \quad (29)$$

$$\overline{\theta} = \frac{\theta_0 - [(1-\alpha)\theta_0 + \alpha\theta_c] f_{HAB}}{\alpha(1 - f_{HAB})}. \quad (30)$$

Hence,

$$\sqrt{\rho_{LAB}} = \sqrt{\frac{2n f_{LAB}\overline{\theta}}{bD}} = \sqrt{\frac{2n\overline{\theta}(1-f_{HAB})}{bD}} = \sqrt{\frac{2n(1-f_{HAB}) \times \frac{\theta_0 - [(1-\alpha)\theta_0 + \alpha\theta_c] f_{HAB}}{\alpha(1-f_{HAB})}}{bD}} = \sqrt{\frac{2n \times \{\theta_0 - [(1-\alpha)\theta_0 + \alpha\theta_c] f_{HAB}\}}{\alpha bD}}. \quad (31)$$

Combined with Eq. (24), we can obtain

$$\tau = Gb\left(A_1\sqrt{\rho_i} + A_2\sqrt{\frac{2n\{\theta_0 - [(1-\alpha)\theta_0 + \alpha\theta_c] f_{HAB}\}}{\alpha bD}}\right). \quad (32)$$

Recall that in this equation, the parameter D is the average crystallite size. Therefore, one can easily see that Eqs. (32) and (23) bear the same form without considering the misorientations. Eq. (32) also suggests that the flow stress decreases when the fraction of HAGBs increases.

Based on the physical processes involved in dislocation mediated plasticity, the associated activation volume can be written as [59,66,80]

$$V^* = b \times l^* \times \xi, \quad (33)$$

where b is the Burgers vector, l^* is the length of dislocation segment involved in the thermal activation, and ξ is the distance swept by the mobile dislocation line during an activation event, and it can be considered as a constant. In addition, two limits of l^* have been suggested [59,66], l_1^* and l_2^*, and

$$l_1^* = \frac{a}{\sqrt{\rho}}. \quad (34)$$

$$l_2^* = \chi d. \quad (35)$$

Here l_1^* is likely to control the length scale when the grain sizes are large and dislocation density is low, whereas, l_2^* is likely to control the length scale when the grain sizes are small. The parameters a and χ are related to the material's properties. From the preliminary model provided in Reference [59], one can easily understand the results of Figure 31. The activation volume V^* can be determined from the grain size and dislocation density. For the ECAE Cu subjected to SPD (equivalent strain >10), there is no further apparent grain size refinement with increased number of ECAE passes, and thus the activation volume V^* should approach a constant value; this is shown in Fig. 3.

Then, according to Eq. (4), the strain rate sensitivity can be expressed using the following when the grain size is reduced to the UFG/nc regime:

$$m = \frac{k_B T}{\tau V^*} = \frac{k_B T}{Gb(A_1\sqrt{\rho_i} + A_2\sqrt{(2n\{\theta_0 - [(1-\alpha)\theta_0 + \alpha\theta_c] f_{HAB}\})/\alpha bD})b \times \xi \times \chi D} = \frac{k_B T}{b \times \xi \times \chi Gb(A_1 D\sqrt{\rho_i} + A_2\sqrt{(2nD\{\theta_0 - [(1-\alpha)\theta_0 + \alpha\theta_c] f_{HAB}\})/\alpha b})}. \quad (36)$$

Eq. (36) indicates that when the grain size is reduced to the UFG/nc regime, there is a tendency of the value of m to increase with further grain size reduction. For the ECAE Cu, however, if the equivalent strain is large enough, the primary deformation mechanism is still the strain induced recrystallization and grain misorientation evolution. Therefore, Eq. (36) gives a reasonable explanation of the observed strain rate sensitivity tendency as shown in Fig. 2.

5.2. Comparison between model predictions and the experimental results

In the construction of the constitutive model, strain hardening, dynamic recovery, and recrystallization have been considered, and the strain rate effect has been coupled with the stress using the creep theory proposed by Sellars and Tegart [58].

In Eq. (17), the strain rate effect and flow stress can be connected by the Zener–Hollomon (Z) parameter. Usually, the parameter α is optimized to obtain the minimum variation of n' by plotting the strain rate against ($sinh\alpha\sigma$) at any given temperature [62]. However, our nanoindentation experiments only provide the results at room temperature and, therefore, we cannot identify the specific values of α and n' via the above method. As such, a simplified form of Eq. (17) has been utilized in this treatment, i.e., Eq. (18).

Based on our nanoindentation results, however, a constitutive model in terms of the material's hardness can be utilized by substituting the strength converted from hardness, and the constitutive model can be rewritten as

$$H_i = \xi_i ln\dot{\varepsilon} + \eta_i. \quad (20b)$$

$$H = H_{sat} + (H_{wh} - H_{sat})\exp\left[-r\left(\frac{\varepsilon}{\varepsilon_p}\right)^q\right] = \xi_{sat}\ln\dot{\varepsilon} + \eta_{sat} + [H_{wh} - (\xi_{sat}\ln\dot{\varepsilon} + \eta_{sat})]\exp\left[-r\left(\frac{\varepsilon}{\varepsilon_p}\right)^q\right]. \quad (21b)$$

$$H_{wh} = \sqrt{H_s^2 + (H_0^2 - H_s^2)exp[-\beta\varepsilon]} = \sqrt{(\xi_s ln\dot{\varepsilon} + \eta_s)^2 + [(\xi_0 ln\dot{\varepsilon} + \eta_0)^2 - (\xi_s ln\dot{\varepsilon} + \eta_s)^2]exp[-\beta\varepsilon]}. \quad (22b)$$

The relation between hardness and the logarithmic strain rate is shown in Fig. 4. From this figure, the value of the parameters ξ_i

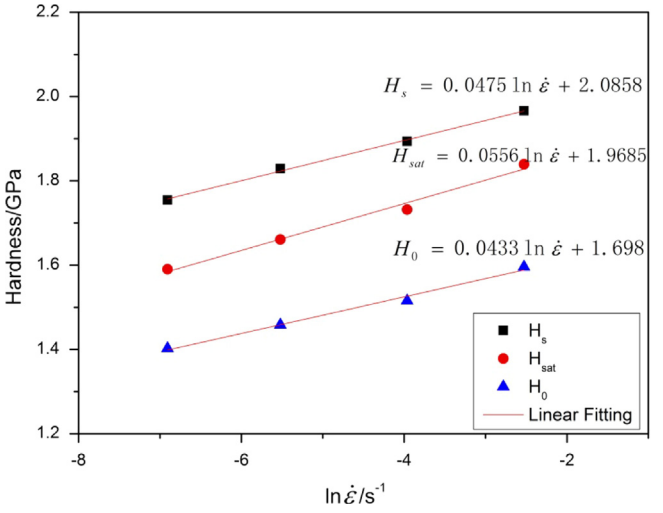

Fig. 4. Hardness as a function of strain rate (the strain rate is plotted in natural logarithm). Also note, in this figure, the H_0 is the initial hardness (zero equivalent strain), which is the hardness value in the as-received condition; H_s represents the hardness value at the peak point; and H_{sat} represents the final saturation hardness value.

Table 1
Parameter values of the ξ_i and η_i at different hardness levels.

	ξ_i	η_i
$i=0(H_0)$	0.0433	1.698
$i=s(H_s)$	0.0475	2.0858
$i=sat(H_{sat})$	0.0556	1.9685

Table 2
Input parameters of the constitutive model.

Parameter	Value
H_0 (MPa)	$H_0=0.0433\ln\dot{\varepsilon}+1.698$
H_s (MPa)	$H_s=0.0475\ln\dot{\varepsilon}+2.0858$
H_{sat} (MPa)	$H_{sat}=0.0556\ln\dot{\varepsilon}+1.9685$
ε_p	5.0
r	0.01
q	3.0
β	2/3

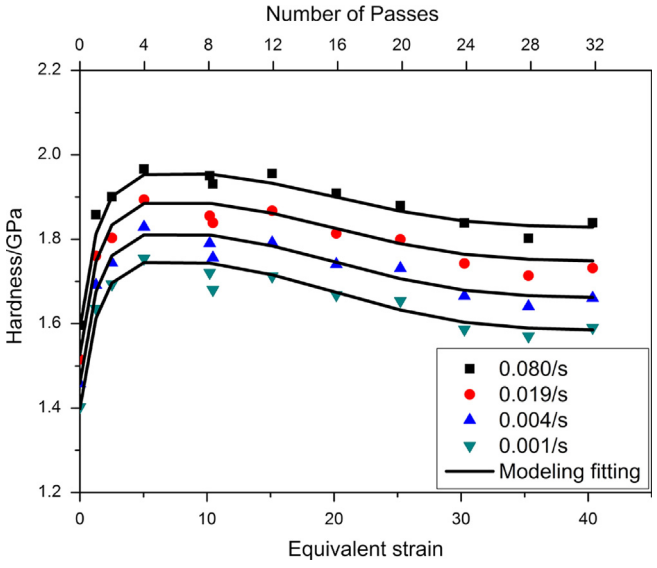

Fig. 5. Comparison between the constitutive model predictions and experimental results. The solid curves are the model predictions. In this figure, the equivalent strain is calculated using the equation proposed in [1,7]; that is, $\varepsilon_N=(N/\sqrt{3})[2\cot((\Phi/2)+(\Psi/2))+\Psi\,\mathrm{cosec}((\Phi/2)+(\Psi/2))]$. There is a very good agreement between the model predictions and the experimental results.

and η_i can be identified, and are listed in Table 1. All other parameters can be obtained by further analysis, and Table 2 gives the reference value of each parameter. With insertion into the constitutive relationship developed and a comparison between the model prediction and experimental results becomes possible. This is displayed in Fig. 5. From the goodness of the fits, it is quite obvious that a good agreement between the model prediction and the experimental results has been obtained. In other words, the constitutive model we have constructed, based on simple physics, successfully captures the essential hardening features of ECAE Cu processed up to 32 passes.

6. Summary and concluding remarks

A strain rate dependent constitutive model of ECAE Cu has been constructed based on the dislocation mechanisms during severe plastic deformation, including accumulation of dislocations, dynamic recovery and recrystallization. A good agreement has been obtained between the model predictions and experimental results.

Based on nanoindentation results, with increased number of ECAE passes or equivalent strain, the strain rate sensitivity has a tendency of continuous increasing, while the activation volume saturates at a constant value when the number of ECAE passes is larger than four. The microstructural evolution, especially the transformation of low angle grain boundaries into high angle grain boundaries causes the decreasing of flow stress, and consequently leads to the increase in strain rate sensitivity. However, the activation volume can only be determined by the grain size when the grain size is small and by the dislocation density when the grain size is large.

Acknowledgments

The authors acknowledge the support from the US Army Research Laboratory for the preparation and supply of specimens. J. Su would like to thank the Chinese Ministry of Education for the support during her stay at UNC-Charlotte, and for the support from China Scholarship Council. Q. Wei is supported by the US Army Research Laboratory under Contract no. W911QX-08-C-0073.

References

[1] R.Z. Valiev, T.G. Langdon, Prog. Mater. Sci. 51 (2006) 881–981.
[2] R.Z. Valiev, Y. Estrin, Z. Horita, T.G. Langdon, M.J. Zechetbauer, Y.T. Zhu, JOM J. Miner. Met. Mater. Soc. 58 (2006) 33–39.
[3] A.P. Zhilyaev, T.G. Langdon, Prog. Mater. Sci. 53 (2008) 893–979.
[4] Y. Estrin, A. Vinogradov, Acta Mater. 61 (2013) 782–817.
[5] V. Segal, Google Patents, 1996.
[6] V. Segal, Mater. Sci. Eng. A 197 (1995) 157–164.
[7] V. Segal, Mater. Sci. Eng. A 271 (1999) 322–333.
[8] V. Segal, Mater. Sci. Eng. A 338 (2002) 331–344.
[9] V. Segal, Mater. Sci. Eng. A 345 (2003) 36–46.
[10] V. Segal, Mater. Sci. Eng. A 386 (2004) 269–276.
[11] V. Segal, Mater. Sci. Eng. A 406 (2005) 205–216.
[12] A. Azushima, R. Kopp, A. Korhonen, D. Yang, F. Micari, G. Lahoti, P. Groche, J. Yanagimoto, N. Tsuji, A. Rosochowski, CIRP Ann.—Manuf. Technol. 57 (2008) 716–735.
[13] R.Z. Valiev, R. Islamgaliev, I. Alexandrov, Prog. Mat. Sci. 45 (2000) 103–189.
[14] Y.T. Zhu, T.C. Lowe, Mater. Sci. Eng. A 291 (2000) 46–53.
[15] R. Valiev, Nat. Mater. 3 (2004) 511–516.
[16] R. Valiev, E. Kozlov, Y.F. Ivanov, J. Lian, A. Nazarov, B. Baudelet, Acta Metall. Mater. 42 (1994) 2467–2475.
[17] A. Vinogradov, T. Ishida, K. Kitagawa, V. Kopylov, Acta Mater. 53 (2005) 2181–2192.
[18] S.T. Adedokun, J. Emerg. Trends Eng. Appl. Sci. (JETEAS) 2 (2011) 360–363.
[19] M. Furukawa, Z. Horita, M. Nemoto, T. Langdon, J. Mater. Sci. 36 (2001) 2835–2843.
[20] M. Furukawa, Y. Iwahashi, Z. Horita, M. Nemoto, T.G. Langdon, Mater. Sci. Eng. A 257 (1998) 328–332.
[21] Q. Wei, L.J. Kecskes, T. Jiao, K.T. Hartwig, K.T. Ramesh, E. Ma, Acta Mater. 52 (2004) 1859–1869.
[22] Q. Wei, T. Jiao, S.N. Mathaudhu, E. Ma, K.T. Hartwig, K.T. Ramesh, Mater. Sci. Eng. A 358 (2003) 266–272.
[23] Q. Wei, T. Jiao, K.T. Ramesh, E. Ma, L.J. Kecskes, L. Magness, R.J. Dowding, V.U. Kazykhanov, R.Z. Valiev, Acta Mater. 54 (2006) 77–87.
[24] Q. Wei, Z.L. Pan, X.L. Wu, B.E. Schuster, L.J. Kecskes, R.Z. Valiev, Acta Mater. 59 (2011) 2423–2436.
[25] Q. Wei, K.T. Ramesh, E. Ma, L.J. Kesckes, R.J. Dowding, V.U. Kazykhanov, R.Z. Valiev, Appl. Phys. Lett. 86 (2005) 101907.
[26] Q. Wei, K.T. Ramesh, B.E. Schuster, L.J. Kecskes, R.J. Dowding, J. Miner. Met. Mater. Soc. 58 (2006) 40–44.
[27] Q. Wei, H. Zhang, B.E. Schuster, K.T. Ramesh, R.Z. Valiev, L.J. Kecskes, R.J. Dowding, Acta Mater. 54 (2006) 4079–4089.
[28] Z. Pan, F. Xu, S.N. Mathaudhu, L.J. Kecskes, W.H. Yin, X.Y. Zhang, K.T. Hartwig, Q. Wei, Acta Mater. 60 (2012) 2310–2323.
[29] C.X. Huang, H.J. Yang, S.D. Wu, Z.F. Zhang, Mater. Sci. Forum 584–586 (2008) 333–337 (Trans Tech Publ.).
[30] X. Molodova, G. Gottstein, M. Winning, R. Hellmig, Mater. Sci. Eng. A 460 (2007) 204–213.
[31] Y. Li, N. Tao, K. Lu, Acta Mater. 56 (2008) 230–241.
[32] A. Mishra, B. Kad, F. Gregori, M. Meyers, Acta Mater. 55 (2007) 13–28.

[33] S. Ferrasse, K.T. Hartwig, R.E. Goforth, V.M. Segal, Metall. Mater. Trans. A 28 (1997) 1047–1057.
[34] S. Ferrasse, V. Segal, S. Kalidindi, F. Alford, Mater. Sci. Eng. A 368 (2004) 28–40.
[35] M. Zehetbauer, T. Ungar, R. Kral, A. Borbely, E. Schafler, B. Ortner, H. Amenitsch, S. Bernstorff, Acta Mater. 47 (1999) 1053–1061.
[36] G.R. Johnson, W.H. Cook, Proceedings of the 7th International Symposium on Ballistics, International Ballistics Committee, The Hague, Netherlands, 1983, pp. 541–547.
[37] F.J. Zerilli, R.W. Armstrong, J. Appl. Phys. 61 (1987) 1816–1825.
[38] P. Follansbee, U. Kocks, Acta Metall. 36 (1988) 81–93.
[39] G.W.-G.S. Nemat-Nasser, Mech. Mater. 35 (2003) 1023–1047.
[40] S. Nemat-Nasser, W. Guo, J. Cheng, Acta Mater. 47 (1999) 3705–3720.
[41] S. Nemat-Nasser, J.B. Isaacs, Acta mater. 45 (1997) 907–919.
[42] R. Liang, A.S. Khan, Int. J. Plasticity 15 (1999) 963–980.
[43] Y. Lin, X.-M. Chen, G. Liu, Mater. Sci. Eng. A 527 (2010) 6980–6986.
[44] G.Z. Voyiadjis, A.H. Almasri, Mech. Mater. 40 (2008) 549–563.
[45] F.H. Abed, G.Z. Voyiadjis, Int. J. Plasticity 21 (2005) 1618–1639.
[46] G.Z. Voyiadjis, F.H. Abed, Mech. Mater. 37 (2005) 355–378.
[47] S. Krishna, S. De, Mech. Mater. 43 (2011) 99–110.
[48] J.-B. Kim, H. Shin, Int. J. Impact Eng. 36 (2009) 746–753.
[49] M.-C. Cai, L.-S. Niu, X.-F. Ma, H.-J. Shi, Mech. Mater. 42 (2010) 774–781.
[50] A. Rusinek, J.A. Rodríguez-Martínez, A. Arias, Int. J. Mech. Sci. 52 (2010) 120–135.
[51] H. Mecking, U. Kocks, Acta Metall. 29 (1981) 1865–1875.
[52] Y. Estrin, H. Mecking, Acta Metall. 32 (1984) 57–70.
[53] W. Wei, K. Wei, G. Fan, Acta Mater. 56 (2008) 4771–4779.
[54] G.Z. Voyiadjis, F.H. Abed, Int. J. Plasticity 22 (2006) 1398–1431.
[55] S. Bodner, Y. Partom, DTIC Document, 1974.
[56] S.F. Medina, C.A. Hernandez, Acta Mater. 44 (1996) 137–148.
[57] C. Zener, J. Hollomon, J. Appl. Phys. 15 (1944) 22–32.
[58] C.M. Sellars, W.J. McTegart, Acta Metall. 14 (1966) 1136–1138.
[59] Q. Wei, S. Cheng, K.T. Ramesh, E. Ma, Mater. Sci. Eng. A 381 (2004) 71–79.
[60] N.Q. Chinh, G. Horváth, Z. Horita, T.G. Langdon, Acta Mater. 52 (2004) 3555–3563.
[61] A. Laasraoui, J.J. Jonas, Metall. Trans. A 22 (1991) 1545–1558.
[62] A. Oudin, M.R. Barnett, P.D. Hodgson, Mater. Sci. Eng. A 367 (2004) 282–294.
[63] E. Shafiei, R. Ebrahimi, ISIJ Int. 52 (2012) 569–573.
[64] R.E. Barber, T. Dudo, P.B. Yasskin, K.T. Hartwig, Scr. Mater. 51 (2004) 373–377.
[65] Y.Z. Guo, N.A. Behm, J.P. Ligda, Y.L. Li, Z. Pan, Z. Horita, Q. Wei, Mater. Sci. Eng. A 586 (2013) 149–159.
[66] Q. Wei, J. Mater. Sci. 42 (2007) 1709–1727.
[67] D. Tabor, Rev. Phys. Technol. 1 (1970) 145–179.
[68] Y. Wang, A. Hamza, E. Ma, Acta Mater. 54 (2006) 2715–2726.
[69] V. Maier, K. Durst, J. Mueller, B. Backes, H.W. Höppel, M. Göken, J. Mater. Res. 26 (2011) 1421–1430.
[70] L. Lu, T. Zhu, Y. Shen, M. Dao, K. Lu, S. Suresh, Acta Mater. 57 (2009) 5165–5173.
[71] J. Chen, Y. Shi, K. Lu, J. Mater. Res. 20 (2005) 2955–2959.
[72] J. Chen, L. Lu, K. Lu, Scr. Mater. 54 (2006) 1913–1918.
[73] Q. Wei, L.J. Kecskes, Mater. Sci. Eng. A 491 (2008) 62–69.
[74] S. Gourdet, F. Montheillet, Acta Mater. 51 (2003) 2685–2699.
[75] R. Doherty, D. Hughes, F. Humphreys, J. Jonas, D.J. Jensen, M. Kassner, W. King, T. McNelley, H. McQueen, A. Rollett, Mater. Sci. Eng. A 238 (1997) 219–274.
[76] S. Gourdet, F. Montheillet, Acta Mater. 50 (2002) 2801–2812.
[77] H. Gleiter, Acta Metall. 17 (1969) 853–862.
[78] F. Dalla Torre, R. Lapovok, J. Sandlin, P. Thomson, C. Davies, E. Pereloma, Acta Mater. 52 (2004) 4819–4832.
[79] L.X. Kong, P.D. Hodgson, B. Wang, J. Mater. Process. Technol. 89–90 (1999) 44–50.
[80] Q. Wei, T. Jiao, K.T. Ramesh, E. Ma, Scr. Mater. 50 (2004) 359–364.